





## Development of an optically gated Fe/*n*-GaAs spin-polarized transistor

J. Y. Kim <sup>1,2</sup> M. Samiepour,<sup>3,\*</sup> E. Jackson <sup>3,†</sup> J. Ryu,<sup>4,‡</sup> D. Iizasa,<sup>4</sup> T. Saito,<sup>4</sup> M. Kohda,<sup>4,5,6</sup>  
J. Nitta <sup>4,5,6</sup> H. E. Beere,<sup>7</sup> D. A. Ritchie,<sup>7</sup> and A. Hirohata <sup>3,§</sup>

<sup>1</sup>*Department of Physics, University of York, York YO10 5DD, United Kingdom*

<sup>2</sup>*Institute of Materials Research and Engineering, Agency for Science,  
Technology and Research (A\*STAR), 138634, Singapore*


<sup>3</sup>*Department of Electronic Engineering, University of York, York YO10 5DD, United Kingdom*

<sup>4</sup>*Department of Materials Science, Tohoku University, Sendai 980-8579, Japan*

<sup>5</sup>*Spintronics Research Network, Tohoku University, Sendai 980-8579, Japan*

<sup>6</sup>*Organisation for Advanced Studies, Center for Science and Innovation in Spintronics (Core Research Cluster),  
Tohoku University, Sendai 980-8579, Japan*

<sup>7</sup>*Department of Physics, University of Cambridge, Cambridge CB3 0HE, United Kingdom*

 (Received 6 February 2022; revised 20 July 2022; accepted 13 September 2022; published 7 October 2022)

Efficient modulation of electrically injected spin signals that is suitable for modern-day transistor functionality is yet to be established. In this work, we demonstrate in detail the fabrication of a Fe/*n*-GaAs spin injection device and the experimental setup for an optical gating of the nonlocal spin transport signal. *In situ* scanning electron microscopy interface imaging reveals more uniform current distribution at the Fe/*n*-GaAs injector interface at bias voltages higher than the Schottky barrier height. Three- and four-terminal Hanle measurements confirm successful spin injection into *n*-GaAs, with strong interfacial spin dephasing at high magnetic fields. A time-resolved pump-probe Kerr rotation setup was used to illuminate circularly polarized light in the region of the pure spin current in Fe/*n*-GaAs lateral spin injection devices, where  $(0.4 \pm 0.3)\%$  modulation of the nonlocal signal depending on the light helicity was observed at 30 K.

DOI: [10.1103/PhysRevB.106.134404](https://doi.org/10.1103/PhysRevB.106.134404)

### I. INTRODUCTION

The spin-polarized field-effect transistor (spin FET) [1] is a critical vehicle to study injection, manipulation, and detection of spin-polarized electrons in a semiconductor. As originally proposed, a two-dimensional electron gas in a semiconductor has been widely exploited as a possible medium for a spin FET due to its high in-plane carrier mobility. In particular, the Fe/GaAs system has been intensely investigated thanks to the very small lattice mismatch, where successful injection and detection of electron spins have been reported [2,3]. Theoretically the Fe/GaAs(001) and Fe/ZnSe(001) interfaces were calculated to achieve a spin polarization of 99% by the coherent tunneling [4]. Experimentally Crooker *et al.* measured the spin polarization of 32% at an Fe/GaAs Schottky junction [5], and also reported distributions in the reversal of spin polarization with respect to the applied bias, which can be caused by spin transport through an interfacial resonant state as theoretically predicted [6]. To avoid such

inconsistency in devices, Fleet *et al.* succeeded to grow an abrupt Fe/GaAs(001) interface epitaxially using cold deposition at  $\sim 173$  K, confirming reproducible spin-polarized current injection without bias-dependent reversal [7]. Using InAs, which forms an almost negligible depletion layer at the interfaces and edges, successful spin injection was also demonstrated at 75 K [8], followed by spin injection into Si [9].

However, modulation of the injected spins via electromagnetic gating is still required to create a working spin FET. Recently electrical field operation has been demonstrated in an InAs quantum well, where  $360^\circ$  rotation in  $1.2 \mu\text{m}$  was achieved at 1.8 K [10], which was not suitable for the device-level miniaturization. This is because of the limitation in a spin-orbit interaction constant, which is unique to a semiconducting material [11]. We have accordingly proposed optical gating to achieve more effective spin modulation in GaAs [12].

In this study, we successfully fabricated four-terminal Fe/*n*-GaAs spin injection devices and performed an optical gating experiment at 30 K. Signs of systematic variation of nonlocal spin voltage depending on the optical gating polarization were observed, indicating nonlocal spin accumulation could be modified with spins of optically injected charge carriers. *In situ* scanning electron microscopy (SEM) interface imaging of the Fe/GaAs injector interface was also used to reveal bias dependence of charge transport uniformity across the injector interface.

\*Present address: Seagate Technology, Londonderry BT48 0LY, United Kingdom.

†Present address: Oxford Instruments, Abingdon OX13 5QX, United Kingdom.

‡Present address: Samsung Advanced Institute of Technology, Suwon 16678, Republic of Korea.

§atsufumi.hirohata@york.ac.uk

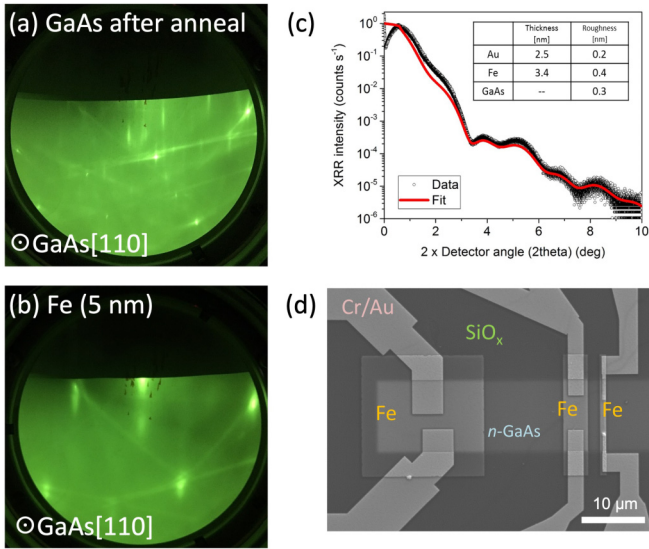


FIG. 1. RHEED (15 keV) images of (a) GaAs(001) after 800 °C anneal and (b) 5-nm deposition of Fe. (c) X-ray reflection measurement of a GaAs/Fe/Au film stack. (d) Scanning electron microscope image of a fabricated four-terminal device.

## II. EXPERIMENTAL PROCEDURES

First, careful design of  $n$ -doped GaAs stacks were required to enable efficient electrical spin injection. The GaAs modulation-doped stacks were grown by molecular beam epitaxy (MBE) in the Semiconductor Physics Group in the University of Cambridge. On a semi-insulating GaAs(001) substrate, 250 nm of GaAs buffer layer was deposited, followed by  $2\ \mu\text{m}$  of lightly doped ( $n = 2 \times 10^{16}\ \text{cm}^{-3}$ , Si dopants)  $n$ -GaAs as the main conducting channel. In order to create sharp Schottky barriers at the Fe/GaAs interface with a narrow ( $< 20\ \text{nm}$ ) depletion region, required for efficient electrical spin injection, further 15 nm of modulation ( $n = 2 \times 10^{16}\ \text{cm}^{-3} \rightarrow 5 \times 10^{18}\ \text{cm}^{-3}$ ) followed by 15 nm of highly doped ( $n = 5 \times 10^{18}\ \text{cm}^{-3}$ ) layer were deposited on top of the channel layer. The sharp,  $\sim 10$ -nm-wide Schottky barrier formation was confirmed using a one-dimensional Poisson/Schrödinger solver [13], as shown in Supplemental Material Sec. I [14]. The stacks were then capped with a  $\sim 300$ -nm-thick amorphous As cap to protect the  $n$ -GaAs surface from oxidation before being transferred to another MBE chamber in York for the epitaxial Fe thin film growth. In the second chamber, the GaAs stack was annealed up to 600 °C to thermally desorb the As cap and prepare the pristine GaAs(001) surface for Fe deposition. Figure 1(a) shows typical reflection high-energy electron diffraction (RHEED) patterns of GaAs(001) surface after the *in situ* annealing, where the sharp streaks indicate highly ordered crystalline GaAs(001) surfaces prior to the Fe deposition. 5 nm of Fe thin films and Au capping layers were then deposited by MBE at room temperature, where the resultant RHEED patterns in Fig. 1(b) indicates the epitaxial growth relation of GaAs(001)[100]/Fe(001)[100]. In Fig. 1(c), x-ray reflection measurement performed on the sample showed the roughness of the crucial Fe/GaAs interface to be less than 0.5 nm.

The device for the nonlocal measurements were then fabricated using three-step electron-beam lithography. First, the Fe thin films were etched using Ar-ion milling into rectangular contacts with  $(1, 4, 20) \times 20\ \mu\text{m}^2$  dimensions, as seen in Fig. 1(d). This process also removes the top 30 nm of the highly doped GaAs layer (except below the Fe contacts), to confine the electrical current in the lightly doped GaAs channel layer. This was followed by chemical etching of the GaAs channel layer using an ammonia-based etchant (as the typical sulphuric acid–hydrogen peroxide etchant was found to also etch the Fe contacts) to create the  $10 \times 100\ \mu\text{m}^2$  GaAs mesa. Without removing resists, a  $\text{SiO}_x$  passivation layer was deposited by plasma-enhanced chemical vapor deposition to isolate the GaAs from the Cr/Au contacts, deposited by thermal evaporation, to contact the Fe contacts electrically.

## III. RESULTS AND DISCUSSION

For a successful test of optical gating, efficient electrical spin injection must be achieved first. In order to test the quality of the Fe/ $n$ -GaAs Schottky barrier at the interface, a three-terminal current-voltage characteristic was measured at 4 K, as seen in Fig. 2(a). At the negative bias between contacts 2 and 4 (i.e., electrons moving from Fe to GaAs), the dc injection current of  $\sim -1\ \text{mA}$  was achieved at around  $-1\ \text{V}$ , as observed similarly in Lou *et al.* [2]. The observed asymmetric  $I$ - $V$  curve across the Fe/GaAs interface is due to the asymmetric nature of the Schottky barrier, where biasing in opposite directions results in different “effective” widths of the Schottky barrier, as also previously observed [2,15].

The quality of the Fe/GaAs spin injection interface is confirmed by nondestructive scanning electron microscopy (SEM) of the buried interface. Figure 2(b) shows a nondestructive SEM image of contacts 1–3 with an injection current  $I_{2-1}$  of  $-125\ \mu\text{A}$ , which was obtained by normalizing the contrast difference between the images taken at 2.5- and 3-kV deceleration voltage of the sample stage (further details can be found in [16]). Deviations in the SEM image contrast of the injector contacts [highlighted by yellow rectangles in Fig. 2(b)] are normalized by the contrast in the drain contacts (highlighted by green rectangles) and are plotted against the injection current  $I_{2-1}$  and the interface voltage  $V_{2-4}$  in Fig. 2(c). As expected, the deviation is the highest for the lowest injection current, where the transport is expected to be nonuniform, and the contrast deviation decreases (i.e., the transport becomes more uniform) as the injection current/interface bias voltage increases enough to overcome the Schottky barrier height. The large drop of the contrast deviation between the  $-200$ - and  $-400$ - $\mu\text{A}$  injection current suggests that the effective height of the Schottky barrier in this device is  $\sim 0.45\ \text{V}$ , roughly in agreement with previously observed values [17,18]. These results confirm the validity of the nondestructive imaging to assess the corresponding transport properties.

The electrical spin injection was characterized using three- and four-terminal Hanle effect measurements at 4 K, as seen in Fig. 2(d). Here the injection current of  $-100\ \mu\text{A}$  was applied between the contacts 2 and 1, while the voltages were measured between the two sets of contacts (2-4) and (3-4), respectively. The application of the out-of-plane magnetic

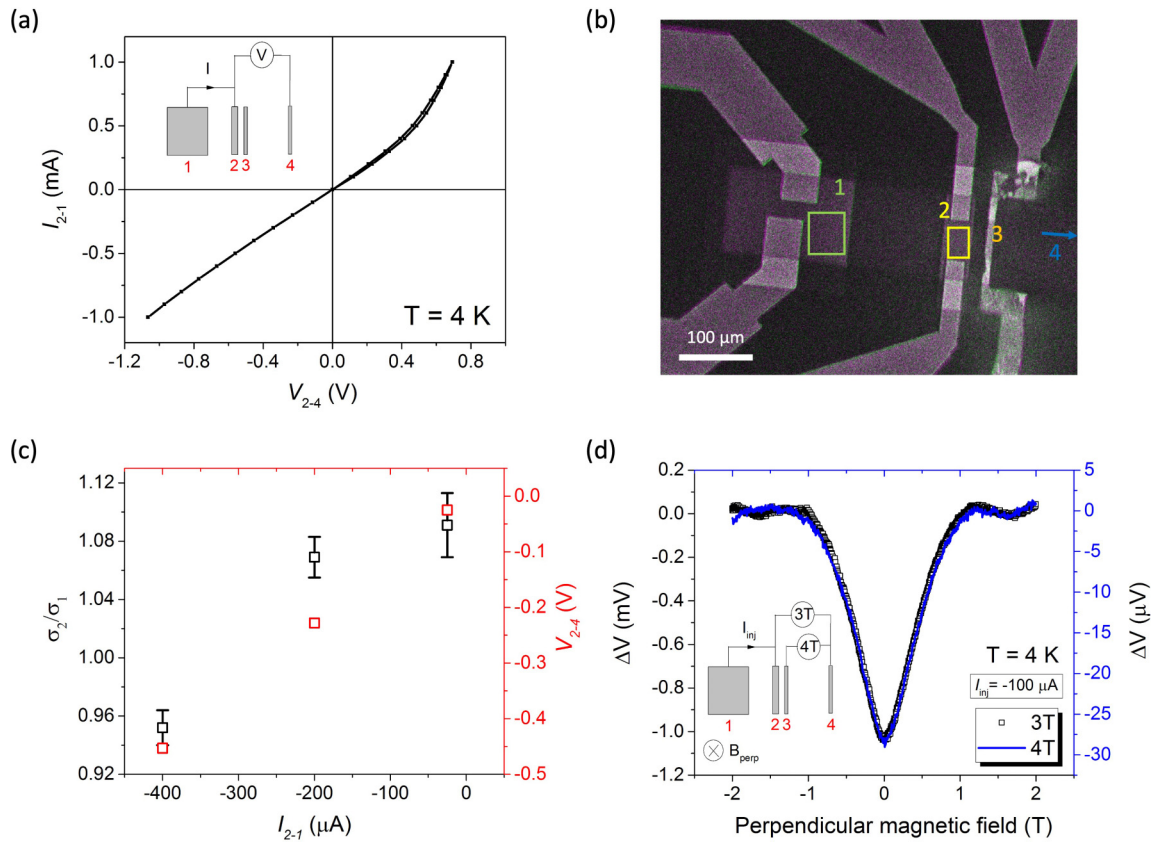


FIG. 2. (a) Three-terminal current-voltage relation of the Fe/GaAs interface of the injection contact (2) as measured at 4 K. (b) *In situ* SEM interface image of the spin-valve device with an injection current  $I_{2-1}$  of  $-125 \mu\text{A}$  where two images with 3.0- and 2.5-kV electron-beam deceleration voltages are subtracted to highlight the interface. The yellow and the green rectangles indicate the regions used for contrast deviation analysis of the injector and drain contact, respectively. (c) The injection current  $I_{2-1}$  dependence of the ratio of contrast deviations between the injector (2) and the drain (1) contact,  $\sigma_2/\sigma_1$ , and the interface voltage  $V_{2-4}$ . (d) Three- and four-terminal Hanle voltages (with offset voltages of  $-0.137$  V and  $-2.32$  mV, respectively) measured with  $-100 \mu\text{A}$  injection current at 4 K.

field causes the precession and the dephasing of the injected spins (polarized in the plane of the contact/surface). This is characterized by the decrease in the measured voltages with the increasing field strength. By fitting the Lorentzian function to the observed peaks, the spin dephasing time  $\tau_s$  can be obtained using the following equation:

$$\tau_s = \frac{\hbar}{g\mu_B B_{z,\text{HWHM}}}, \quad (1)$$

where  $g$  factor  $g$  of  $n$ -GaAs is assumed to be  $-0.44$  [19] and  $B_{z,\text{HWHM}}$  is the measured half width at half maximum from the Hanle peak. A strong in-plane magnetic anisotropy of the Fe strip, required for applying the standard Hanle transport model, was verified using superconducting quantum interference device magnetometry in Supplemental Material Sec. II [14]. From the measured half width at half maximum of around 440 mT, the spin dephasing is estimated to be 60 ps in our case. This compares with the previously measured spin lifetime of 24 ns at 10 K [2,20], where the short spin dephasing time seen in our Hanle measurement is attributed to the fast dephasing of the carrier spins in the highly doped ( $n = 5 \times 10^{18} \text{ cm}^{-3}$ ) GaAs layer, as seen in Tran *et al.* [21].

In order to investigate further the spin dephasing time in the  $n$ -GaAs channel, time-resolved Kerr pump-probe measurements were performed at 30 K. A wavelength-tunable

mode-locked pulsed laser with a photoelastic modulator was used to illuminate a circularly polarized beam to the  $n$ -GaAs channel, while the time-resolved linearly polarized light was used to measure the Kerr response of the channel. Figure 3(a) shows the wavelength dependence of the time-resolved Kerr rotation (TRKR) signal with the applied in-plane magnetic field of 0.65 T at 30 K. The maximum response was observed at around the wavelength of 822 nm, which corresponds well with the 1.5-eV band gap of GaAs expected at 30 K [22]. The precession and the dephasing of the optically injected spins from the Kerr signal at time  $\Delta t$  after the initial excitation can be modeled using the following equation [23]:

$$S_z = S_0 \exp(-\Delta t/\tau_s) \cos(\Omega \Delta t), \quad (2)$$

where  $S_0$  is the initial spin moment (at  $\Delta t = 0$ ), and  $\Omega$  is the precession frequency of the injected spins. The numerical fitting of the Kerr response at the 822-nm excitation wavelength gives the spin dephasing time  $\tau_s$  of  $\sim 2.7$  ns at 30 K, which is in agreement with the literature values [2,23]. The large discrepancy between the two spin dephasing times obtained from the electrical Hanle and the optical TRKR measurements is thought to be due to the dephasing of the electrically injected spins in the “thickness direction.” In order to circumvent this issue, a thinner (800 nm instead of  $2 \mu\text{m}$ ) layer of the GaAs channel could be used, as employed by Shioyai *et al.* [24].

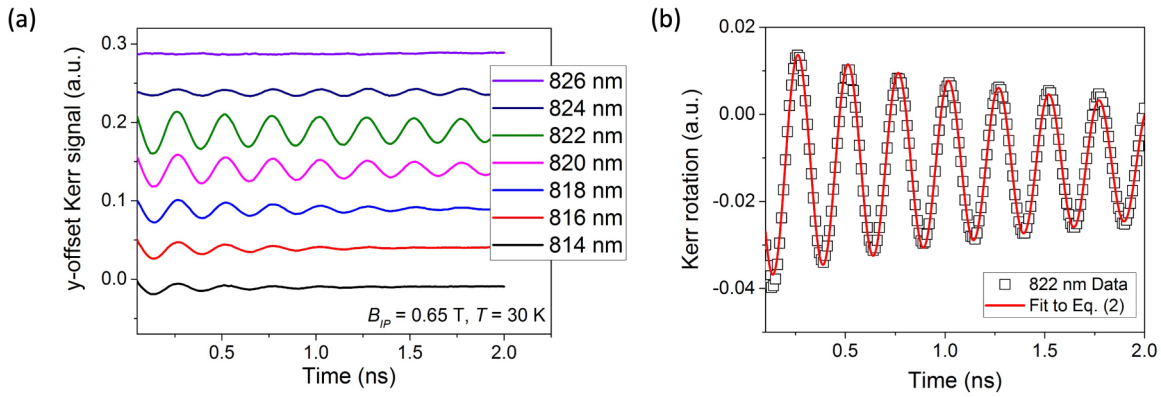


FIG. 3. (a) Wavelength dependence of time-resolved Kerr rotation signals in *n*-GaAs at 30 K. (b) Numerical fit of 822-nm Kerr response to Eq. (2).

In fact, for Si, it is shown that a very thin (70 nm) channel thickness led to a higher spin accumulation possibly due to the confinement of injected spins [25]. To eliminate further spurious sources of the field-dependent signals, nonmagnetic metals could be used as the source and the drain contacts for the nonlocal injection and detection [26].

As the key step to test the feasibility of the optical gating of the nonlocal spin transport, the circularly polarized light at the 822-nm wavelength was illuminated to the region of pure spin current between the injector and the detector ferromagnets as shown in Fig. 4(a). This is similar to the conventional electric

field gate applications of the Datta-Das-type spin field-effect transistor [1,27], where instead of the electric field the circularly polarized light is used to modulate the nonlocal voltage. Figure 4(b) shows the optical micrograph of the spin injection device, where the red circle indicates the region of the nonlocal spin transport where the circularly polarized light was illuminated. Figure 4(c) shows the dependence of the nonlocal voltage measured between contacts 3 and 4, with different laser power and the polarization of the modulation light, measured at 30 K. Systematic differences in the nonlocal transport signal between the cases of the clockwise (red) and the

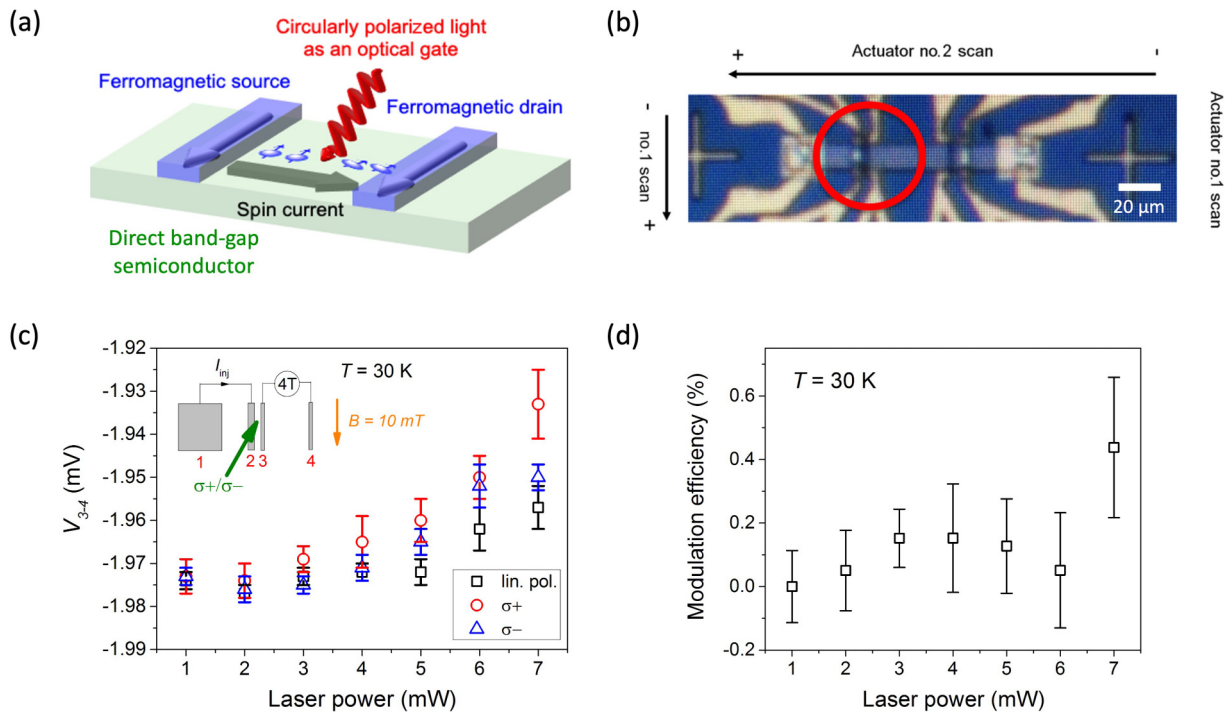


FIG. 4. (a) Schematic of the optical gating in nonlocal spin injection devices. (b) The optical micrograph of our device in the optical cryostat used for the time-resolved Kerr measurements. The red circle indicates the region of the circularly polarized light excitation. (c) Nonlocal voltage (measured between the contacts 3 and 4 with  $I_{inj} = -100 \mu A$  at 30 K) with the clockwise (red) and the counterclockwise (blue) circular polarizations and the linear polarization (black). (d) Optical modulation efficiency, defined as the percentage ratio of the difference and the sum of the nonlocal voltages with the clockwise and the counterclockwise circular polarization,  $(V_{3-4,\sigma+} - V_{3-4,\sigma-}) / (V_{3-4,\sigma+} + V_{3-4,\sigma-})$ , against the laser power.



counterclockwise (blue) circular polarization start to appear with increasing laser power. This is better seen in Fig. 4(d), where the ratio of the difference and the sum of the signals with the two opposite polarizations,  $(V_{\sigma+} - V_{\sigma-})/|(V_{\sigma+} + V_{\sigma-})|$ , is plotted against the laser power. At 7-mW laser power, the ratio, which can be regarded as the optical modulation efficiency, reaches  $(0.4 \pm 0.3)\%$ . This indicates that the spins of the photoexcited carriers are sufficient to modify the accumulation underneath the detector contact directly. This efficiency is comparable to  $\sim 1\%$  modulation efficiency obtained at 2 K by Koo *et al.* [27] via electric-field gating in NiFe/InAs structure, and could increase further with a higher laser power at lower temperatures. Due to the vectorial nature of our gating scheme, where the measured signal depends on the relative angle between the detector magnetization and the accumulated spin polarization, an oscillatory behavior with the light intensity is expected. However, the small differential signals compared with the measurement errors rule out a conclusive observation of the effect at this stage. As can be seen from the large modulation efficiency of the Ampère-field-generating current gating of a nanometric nanoring [28], the miniaturization of our devices is expected to increase our modulation efficiency. The optical gating technique in our structure could have a significant advantage over conventional electric-field gating due to a lower power consumption up to 25% [29].

In the current configuration, the laser spot size was measured to be  $\sim 20 \mu\text{m}$  in diameter, which is almost the same as the GaAs mesa width, and around ten times larger the GaAs area between the Fe electrodes. By tuning the spot size, the efficiency can be enhanced further. In addition, both the spot size and the GaAs mesa can be reduced with maintaining the efficiency, which paves a way towards a nanometric spin FET. This cannot be achieved using the conventional electric and magnetic gating.

#### IV. CONCLUSION

We have successfully demonstrated efficient optical gating on electrical spins injected in Fe/*n*-GaAs with narrow Schottky barriers. Contrast variation analysis of the *in situ* SEM interfacing images allows noninvasive probing of the injector interface uniformity. Three- and four-terminal Hanle measurements reveal the fast spin dephasing time in the highly doped *n*-GaAs layer at high magnetic fields. Time-resolved pump-probe Kerr rotation measurement was performed to demonstrate the optically injected spins in the lightly doped *n*-GaAs channel layer where the highest excitation was observed at 822 nm at 30 K. Helicity-dependent variation of nonlocal signal with optical gating is observed with the modulation efficiency of  $(0.4 \pm 0.3)\%$  at 30 K, which may increase further with higher laser power at lower temperature. Due to the controllability of optical spot size, this method can offer efficient gating in the nanometric scale, which has not been achieved with the conventional electric and magnetic gating.

#### ACKNOWLEDGMENTS

This work was partially supported by the EPSRC program (Grant No. EP/M02458X/1) and JST PRESTO and CREST (Grant No. JPMJCR17J5). J.-Y.K. acknowledges the JSPS Core-to-Core program for the research visits to Tohoku University, the Deutsche Forschungsgemeinschaft (DFG, German Research Foundation), Grant No. TRR 173–268565370 (Project No. B02), the Singapore National Research Foundation Competitive Research Programs (Grant No. NRF-CRP24-2020-0002), and Singapore Agency for Science, Technology and Research (A\*STAR) Science and Engineering Research Council (Grant No. SC25/21-7078D1).

- 
- [1] S. Datta and B. Das, Electronic analog of the electro-optic modulator, *Appl. Phys. Lett.* **56**, 665 (1990).
  - [2] X. Lou, C. Adelman, S. A. Crooker, E. S. Garlid, J. Zhang, K. S. M. Reddy, S. D. Flexner, C. J. Palmström, and P. A. Crowell, Electrical detection of spin transport in lateral ferromagnet–semiconductor devices, *Nat. Phys.* **3**, 197 (2007).
  - [3] G. Salis, A. Fuhrer, R. R. Schlittler, L. Gross, and S. F. Alvarado, Temperature dependence of the nonlocal voltage in an Fe/GaAs electrical spin-injection device, *Phys. Rev. B* **81**, 205323 (2010).
  - [4] O. Wunnicke, Ph. Mavropoulos, R. Zeller, P. H. Dederichs, and D. Grundler, Ballistic spin injection from Fe(001) into ZnSe and GaAs, *Phys. Rev. B* **65**, 241306(R) (2002).
  - [5] S. A. Crooker, Imaging spin transport in lateral ferromagnet/semiconductor structures, *Science* **309**, 2191 (2005).
  - [6] S. Honda, H. Itoh, J. Inoue, H. Kurebayashi, T. Trypiniotis, C. H. W. Barnes, A. Hirohata, and J. A. C. Bland, Spin polarization control through resonant states in an Fe/GaAs Schottky barrier, *Phys. Rev. B* **78**, 245316 (2008).
  - [7] L. R. Fleet, K. Yoshida, H. Kobayashi, Y. Kaneko, S. Matsuzaka, Y. Ohno, H. Ohno, S. Honda, J. Inoue, and A. Hirohata, Correlating the interface structure to spin injection in abrupt Fe/GaAs(001) films, *Phys. Rev. B* **87**, 024401 (2013).
  - [8] P. R. Hammar, B. R. Bennett, M. J. Yang, and M. Johnson, Observation of Spin Injection at a Ferromagnet-Semiconductor Interface, *Phys. Rev. Lett.* **83**, 203 (1999).
  - [9] B. T. Jonker, G. Kioseoglou, A. T. Hanbicki, C. H. Li, and P. E. Thompson, Electrical spin-injection into silicon from a ferromagnetic metal/tunnel barrier contact, *Nat. Phys.* **3**, 542 (2007).
  - [10] W. Y. Choi, H. Kim, J. Chang, S. H. Han, H. C. Koo, and M. Johnson, Electrical detection of coherent spin precession using the ballistic intrinsic spin Hall effect, *Nat. Nanotechnol.* **10**, 666 (2015).
  - [11] A. Hirohata, K. Yamada, Y. Nakatani, I.-L. Prejbeanu, B. Diény, P. Pirro, and B. Hillebrands, Review on spintronics: principles and device applications, *J. Magn. Magn. Mater.* **509**, 166711 (2020).
  - [12] *Spin Current*, 2nd ed., edited by S. Maekawa, S. O. Valenzuela, and E. Saitoh (Oxford University Press, Oxford, 2017).
  - [13] G. L. Snider, I.-H. Tan, and E. L. Hu, Electron states in mesa-etched one-dimensional quantum well wires, *J. Appl. Phys.* **68**, 2849 (1990).

- [14] See Supplemental Material at <http://link.aps.org/supplemental/10.1103/PhysRevB.106.134404> for additional details on 1D band diagrams of interface and a comparison of Fe contact out-of-plane anisotropic magnetoresistance with Hanle data.
- [15] S. Sinha, S. Kumar Chatterjee, J. Ghosh, and A. Kumar Meikap, Semiconducting selenium nanoparticles: Structural, electrical characterization, and formation of a back-to-back Schottky diode device, *J. Appl. Phys.* **113**, 123704 (2013).
- [16] E. Jackson, Y. Wu, W. Frost, J.-Y. Kim, M. Samiepour, K. Elphick, M. Sun, T. Kubota, K. Takanashi, T. Ichinose, S. Mizukami, and A. Hirohata, Non-destructive imaging for quality assurance of magnetoresistive random-access memory junctions, *J. Phys. D: Appl. Phys.* **53**, 014004 (2019).
- [17] H. Kurebayashi, S. J. Steinmuller, J. B. Laloë, T. Trypiniotis, S. Easton, A. Ionescu, J. R. Yates, and J. A. C. Bland, Initial/final state selection of the spin polarization in electron tunneling across an epitaxial Fe/GaAs(001) interface, *Appl. Phys. Lett.* **91**, 102114 (2007).
- [18] L. R. Fleet, H. Kobayashi, Y. Ohno, J.-Y. Kim, C. H. W. Barnes, and A. Hirohata, Interfacial structure and transport properties of Fe/GaAs(001), *J. Appl. Phys.* **109**, 07C504 (2011).
- [19] M. Oestreich and W. W. Rühle, Temperature Dependence of the Electron Landé  $g$  Factor in GaAs, *Phys. Rev. Lett.* **74**, 2315 (1995).
- [20] S. H. Nam, T.-E. Park, Y. H. Park, H.-I. Ihm, H. C. Koo, H. Kim, S. H. Han, and J. Chang, Spin accumulation at in-situ grown Fe/GaAs(100) Schottky barriers measured using the three- and four-terminal methods, *Appl. Phys. Lett.* **109**, 122409 (2016).
- [21] M. Tran, H. Jaffrès, C. Deranlot, J.-M. George, A. Fert, A. Miard, and A. Lemaître, Enhancement of the Spin Accumulation at the Interface between a Spin-Polarized Tunnel Junction and a Semiconductor, *Phys. Rev. Lett.* **102**, 036601 (2009).
- [22] M. B. Panish and H. C. Casey, Temperature dependence of the energy gap in GaAs and GaP, *J. Appl. Phys.* **40**, 163 (1969).
- [23] J. M. Kikkawa and D. D. Awschalom, Resonant Spin Amplification in  $n$ -Type GaAs, *Phys. Rev. Lett.* **80**, 4313 (1998).
- [24] J. Shiogai, M. Ciorga, M. Utz, D. Schuh, M. Kohda, D. Bougeard, T. Nojima, J. Nitta, and D. Weiss, Giant enhancement of spin detection sensitivity in (Ga,Mn)As/GaAs Esaki diodes, *Phys. Rev. B* **89**, 081307(R) (2014).
- [25] A. Spiesser, H. Saito, Y. Fujita, S. Yamada, K. Hamaya, S. Yuasa, and R. Jansen, Giant Spin Accumulation in Silicon Nonlocal Spin-Transport Devices, *Phys. Rev. Appl.* **8**, 064023 (2017).
- [26] L.-K. Liefelth, R. Tholapi, M. Hänze, R. Hartmann, T. Slobodskyy, and W. Hansen, Influence of thermal annealing on the spin injection and spin detection through Fe/GaAs interfaces, *Appl. Phys. Lett.* **108**, 212404 (2016).
- [27] H. C. Koo, J. H. Kwon, J. Eom, J. Chang, S. H. Han, and M. Johnson, Control of spin precession in a spin-injected field effect transistor, *Science* **325**, 1515 (2009).
- [28] B. A. Murphy, A. J. Vick, M. Samiepour, and A. Hirohata, Highly efficient spin-current operation in a Cu nano-ring, *Sci. Rep.* **6**, 37398 (2016).
- [29] A. Hirohata, Spin polarization transistor element, United States Patent US 9,190,500 B2 (17 November 2015).